Electronic Supplementary Material (ESI) for Photochemical & Photobiological Sciences.

Supporting Information

Sequential detection of $Fe^{3+/2+}$ and pyrophosphate by a colorimetric chemosensor in a near-perfect aqueous solution

Ju Byeong Chae, Hyo Jung Jang, Cheal Kim*

Department of Fine Chemistry and Department of Interdisciplinary Bio IT Materials, Seoul National University of Science and Technology, Seoul 139-743, Republic of Korea. Fax: +82-2-973-9149; Tel: +82-2-970-6693; E-mail: chealkim@seoultech.ac.kr

Table S1. Examples for the sequential detection of Fe^{3+} and PPi by organic colorimetric chemosensors.

Sensor	Detection limit of Fe^{3+}	Detection limit of PPi (μM)	Percent of water in solution (%)	Method of detection	Reference
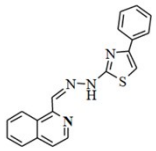	-	-	70	Naked eye	[1]
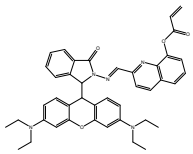	15 nM	0.071	70	Naked eye	[2]
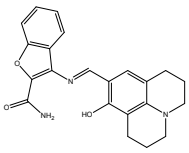	0.36 μM	14.16	99.7	Naked eye	This work

References

1 W. Wang, J. Wei, H. Liu, Q. Liu, Y. Gao, A novel colorimetric chemosensor based on quinoline for the sequential detection of Fe^{3+} and PPi in aqueous solution, *Tetrahedron Lett.* **2017**, *58*, 1025–1029.

2 Z. Li, H. Li, C. Shi, M. Yu, L. Wei, Z. Ni, Nanomolar colorimetric quantitative detection of Fe^{3+} and PPi with high selectivity, *Spectrochim. Acta Part A* **2016**, 159, 249–253.

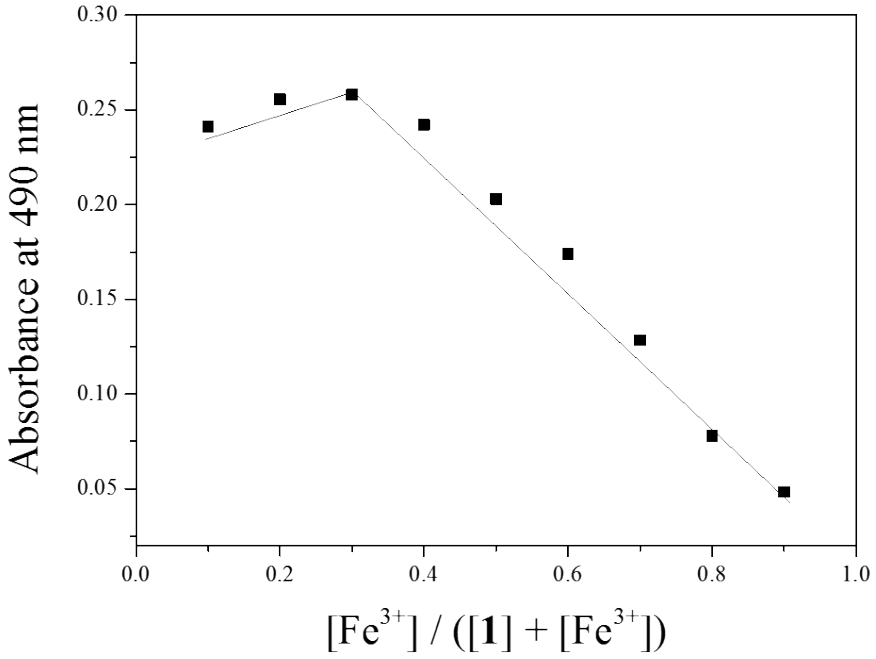

Fig. S1. Job plot of **1** (40 μM) toward Fe^{3+}, where the absorbance at 490 nm was plotted against the mole fraction of Fe^{3+}.

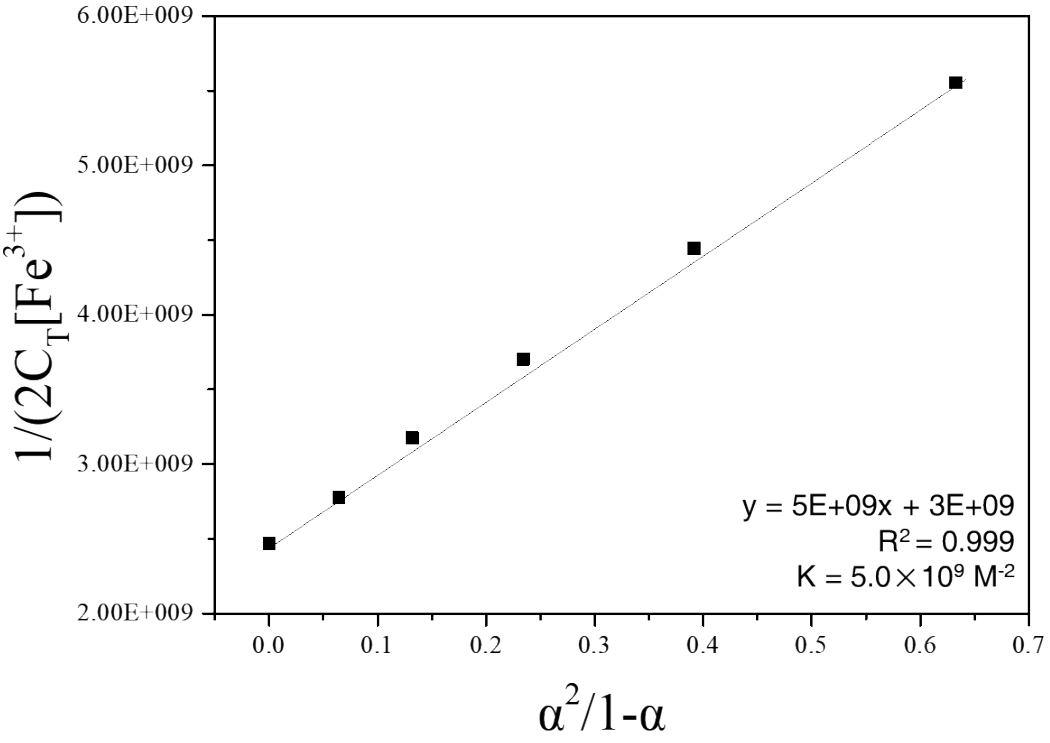

Fig. S2. Li's equation of **1** (30 μM) for Fe^{3+}, assuming 2:1 stoichiometry for association of **1** with Fe^{3+}.

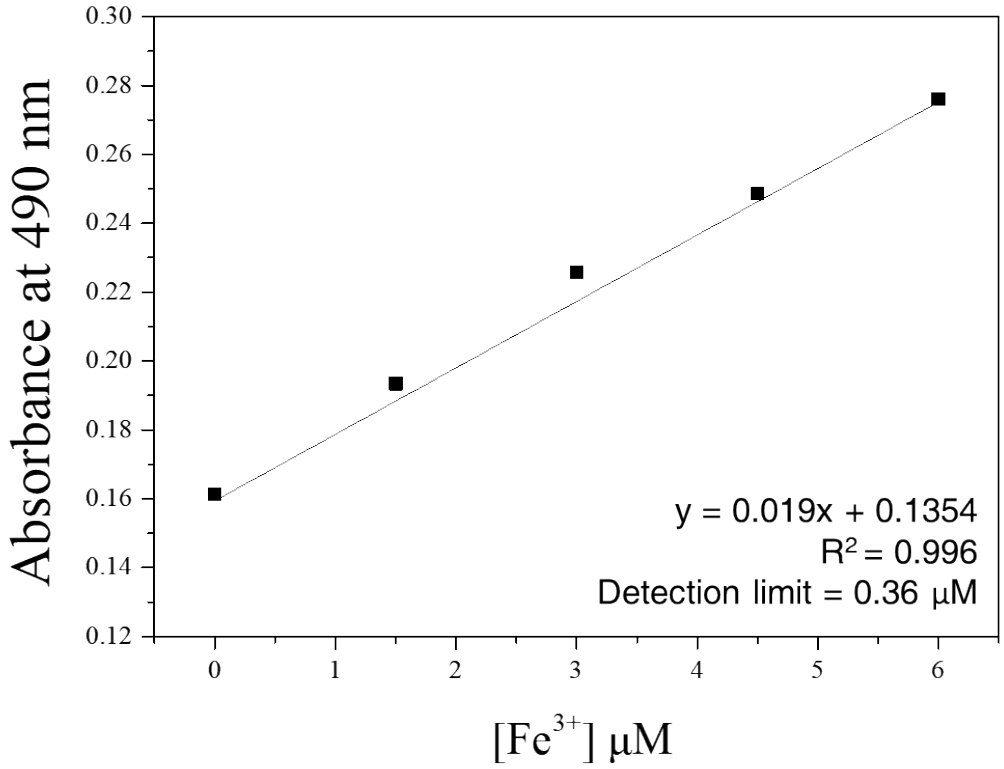

Fig. S3. Determination of the detection limit of **1** (30 μM) for Fe^{3+} based on change of absorbance at 490 nm.

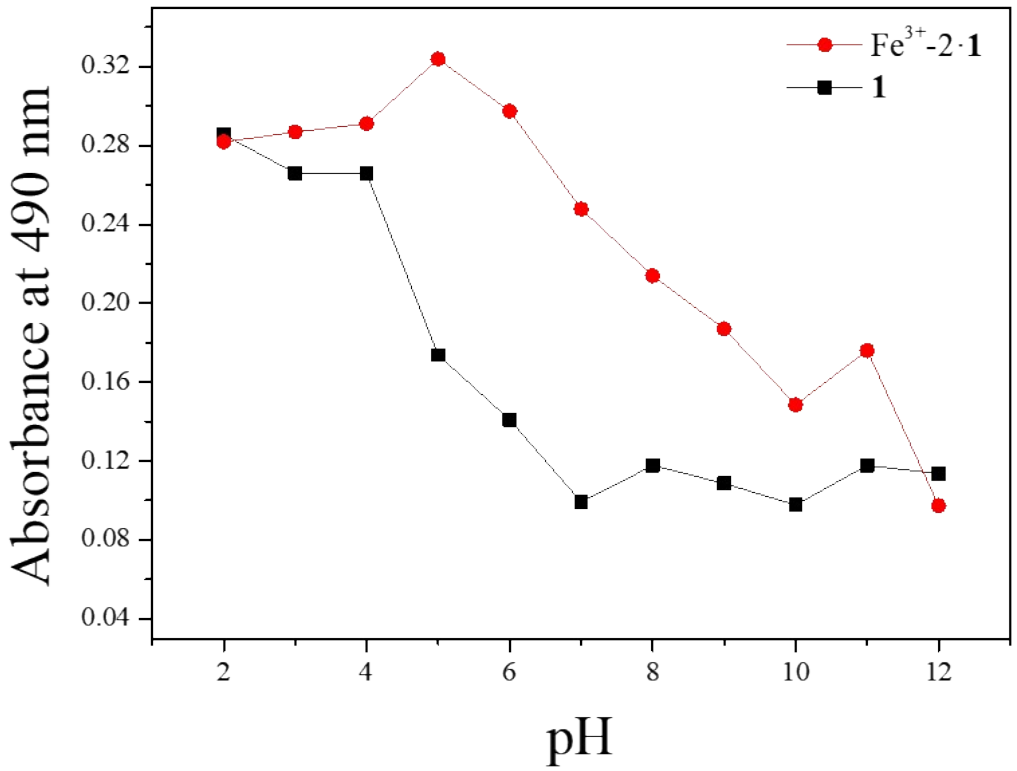

Fig. S4. UV-vis absorbance (at 490 nm) of **1** (30 μM) and Fe^{3+}-2·**1** complex, respectively, in different pH (2-12) solution (bis-tris buffer, 10 mM).

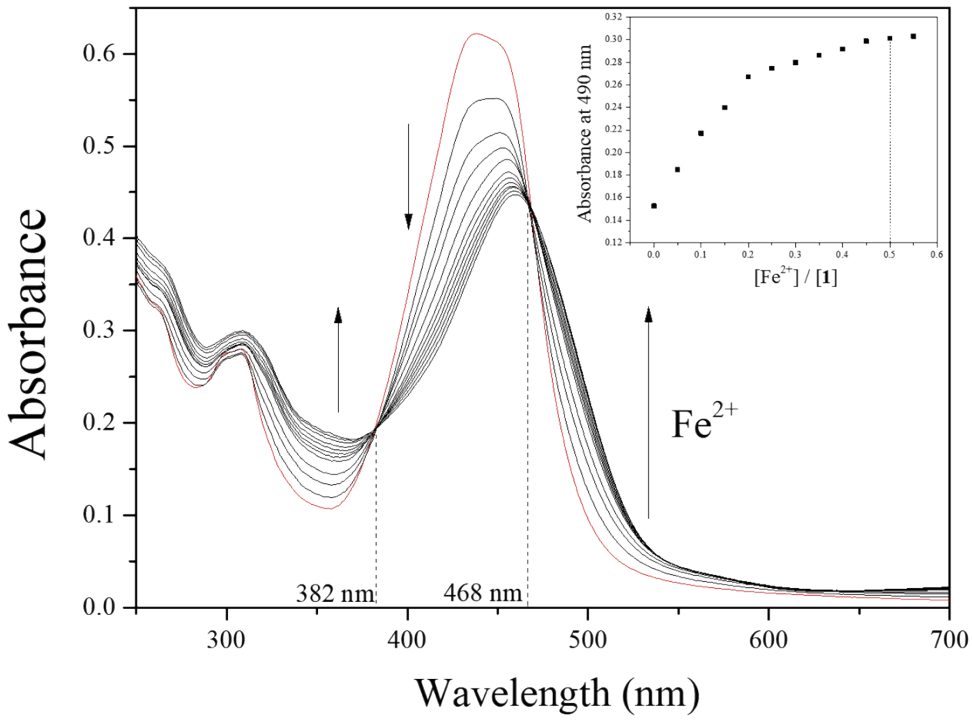

Fig. S5. UV-vis absorption change of **1** (30 μM) with Fe^{2+} ions (0-0.55 equiv) in bis-tris buffer (10 mM, pH = 7.0). Inset : Plot of the absorbance at 490 nm as a function of Fe^{2+} concentration.

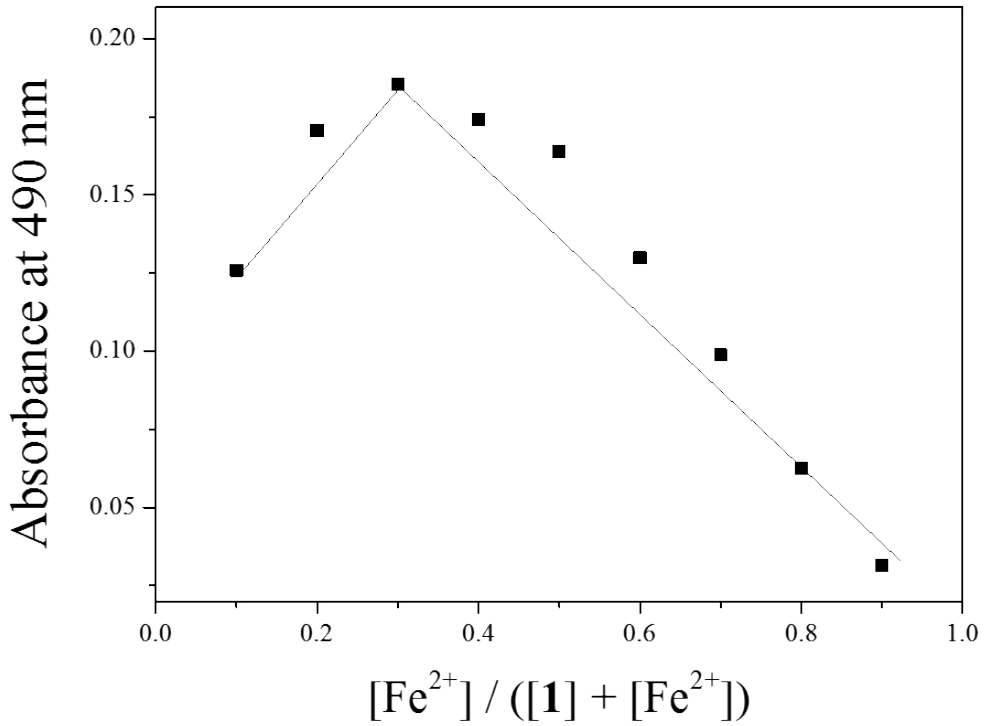

Fig. S6. Job plot of **1** (40 μM) toward Fe^{2+}, where the absorbance at 490 nm was plotted against the mole fraction of Fe^{2+}.

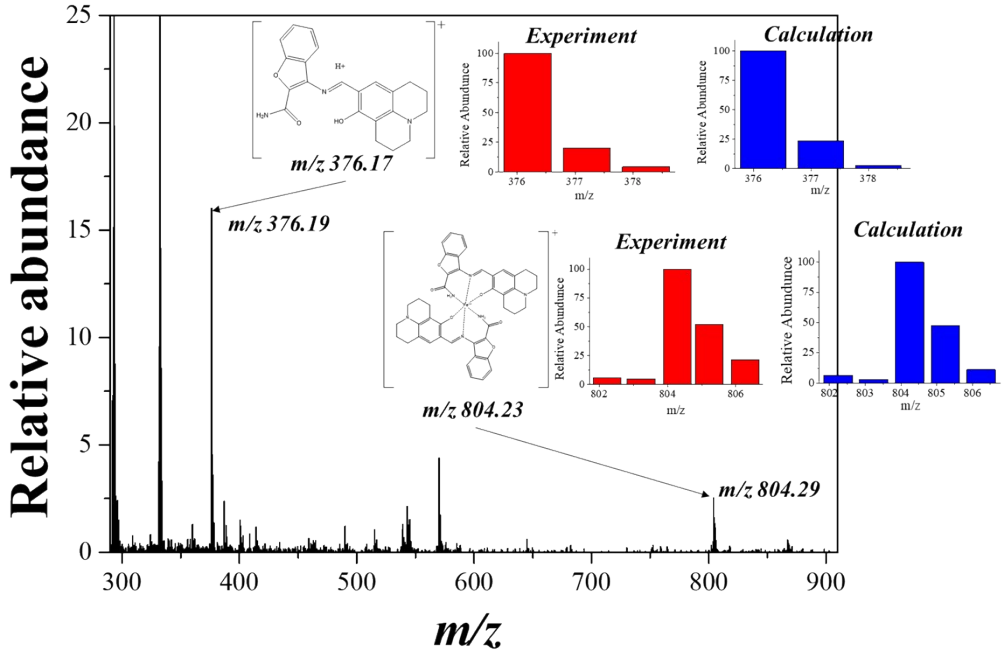

Fig. S7. Positive-ion ESI-mass spectrum of **1** (100 μM) upon addition of 0.5 equiv of Fe^{2+}.

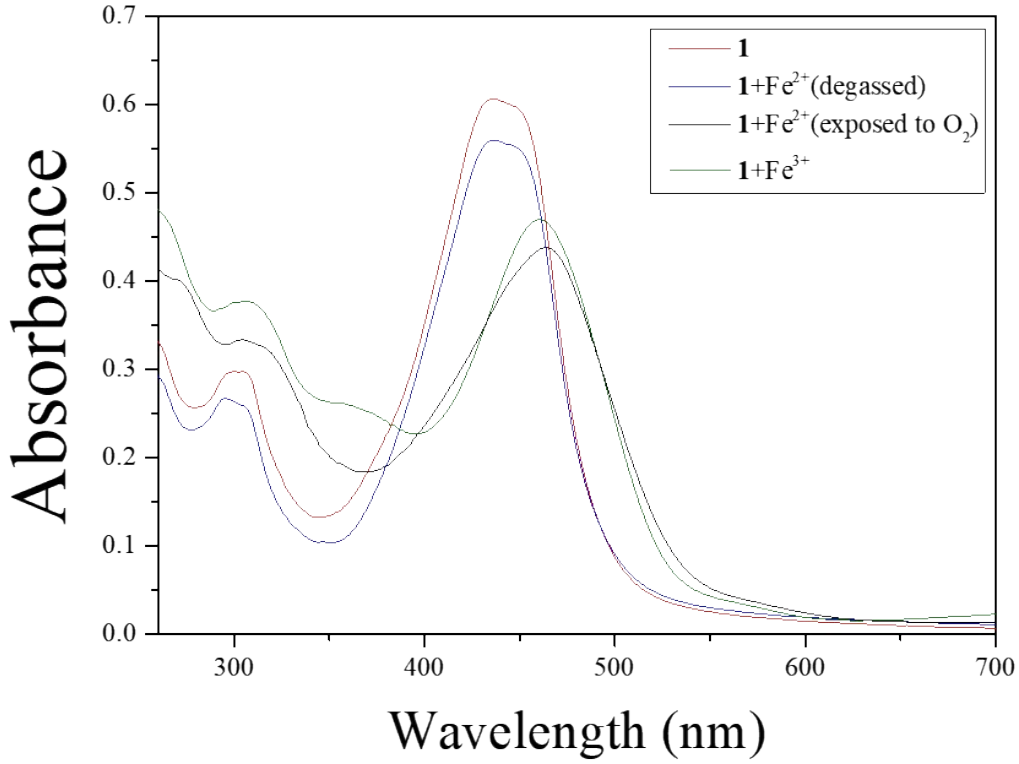

Fig. S8. Absorption spectra of **1** (30 μM) with Fe^{2+} (0.5 equiv) under the degassed and oxygenic conditions, and **1** with Fe^{3+} under the oxygenic conditions.

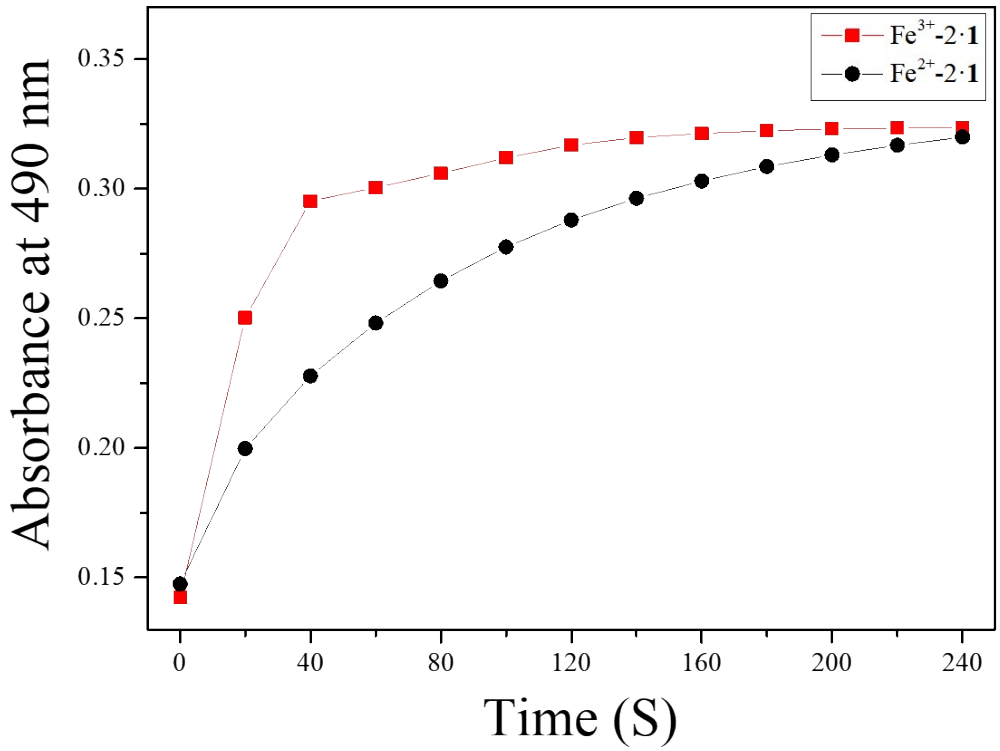

Fig. S9. Formation rates (at 490 nm) of Fe^{3+}-2·**1** complex obtained from the reactions of **1** (30 μM) with $Fe^{3+/2+}$ (0.5 equiv).

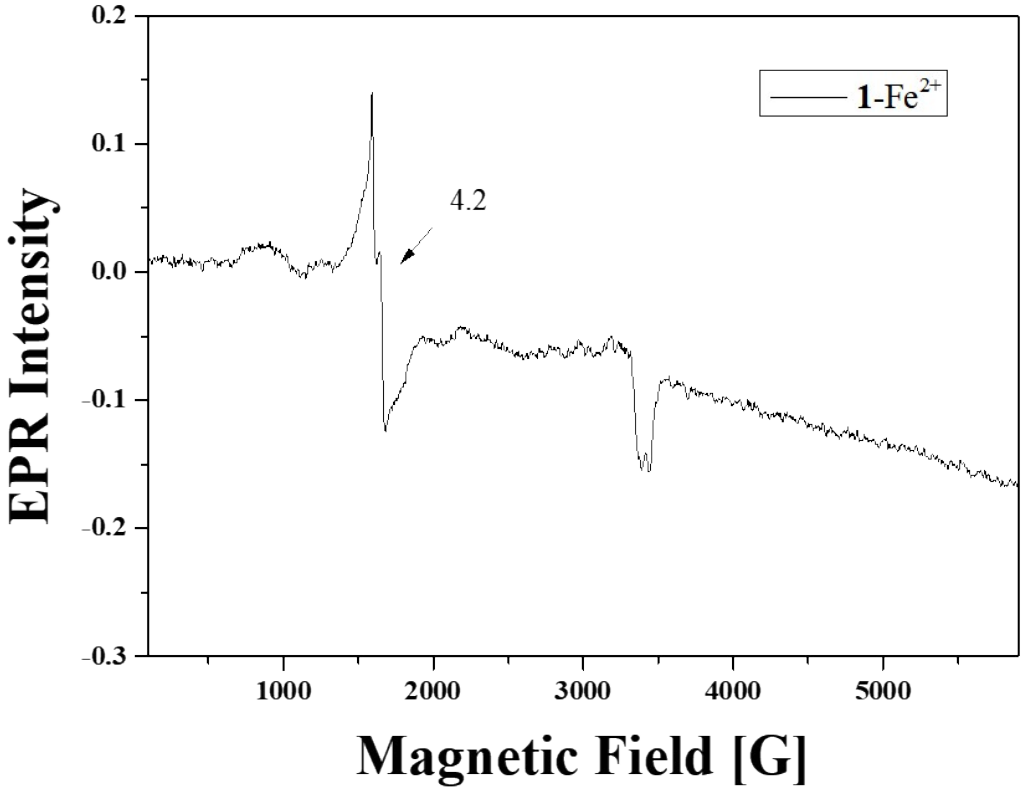

Fig. S10. X-band EPR spectra of Fe^{2+}-2·**1** complex recorded at 4 K. The EPR sample was frozen in liquid nitrogen 10 min after sensor **1** with $Fe(ClO_4)_2$ was mixed in 10 mM bis-tris buffer at room temperature. The experimental parameters: microwave frequency = 9.64 GHz, modulation frequency = 100 kHz, microwave power = 1.0 mW, modulation amplitude = 10 G.

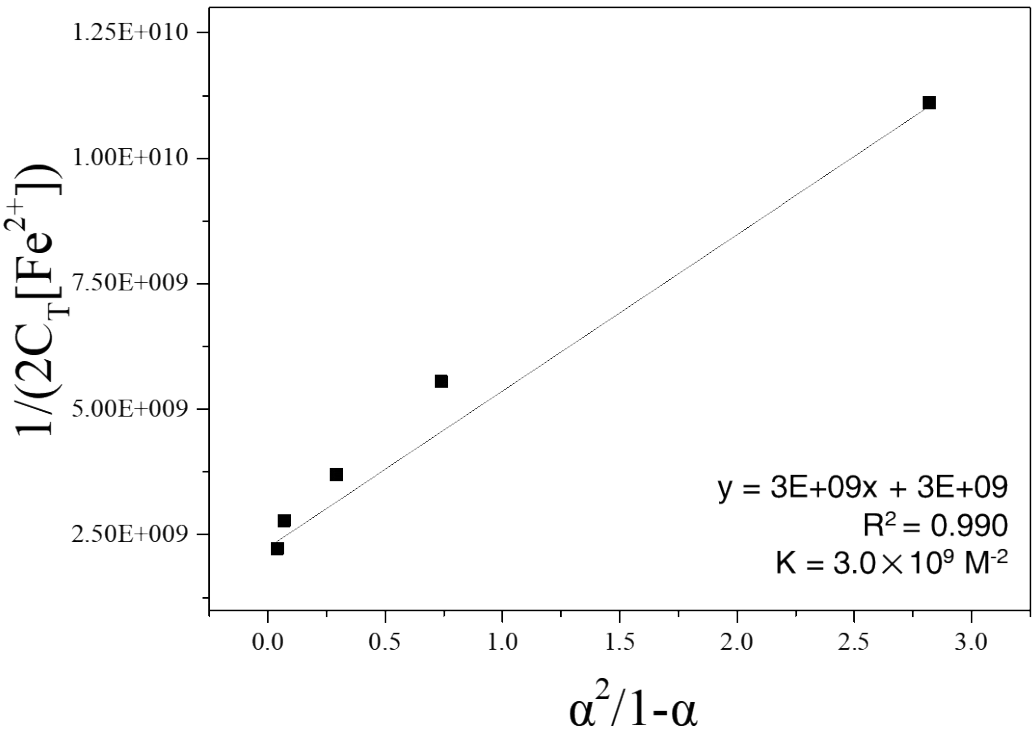

Fig. S11. Li's equation of **1** (30 μM) for Fe^{2+}, assuming 2:1 stoichiometry for association of **1** with Fe^{2+}.

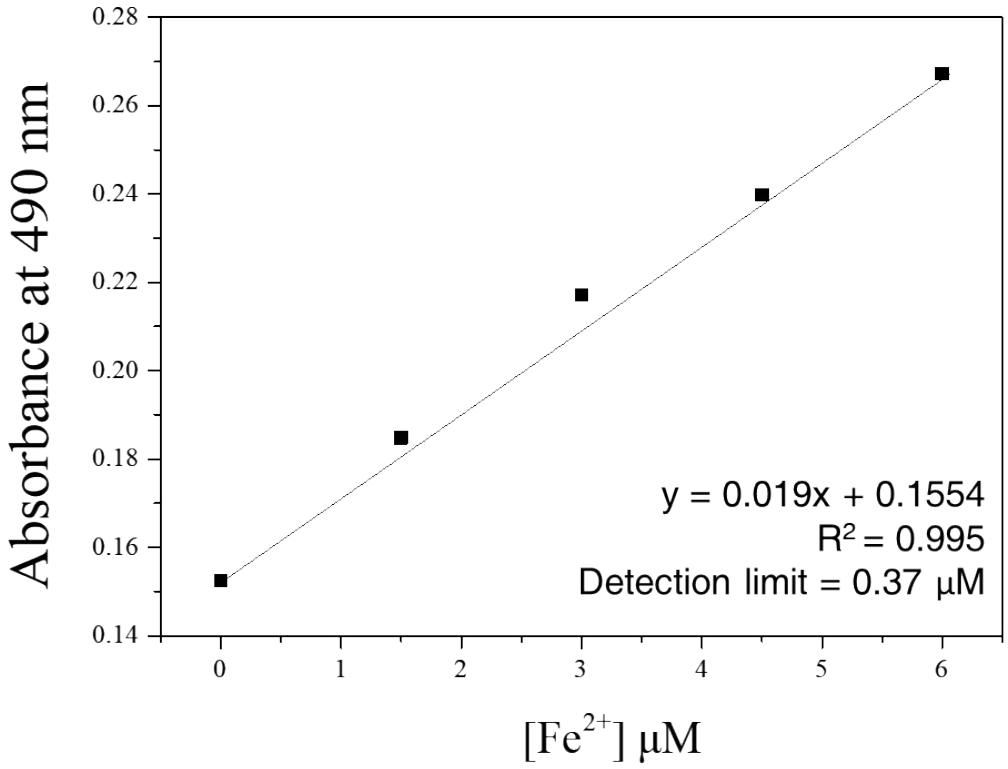

Fig. S12. Determination of the detection limit of **1** (30 μM) for Fe^{2+} based on change of absorbance at 490 nm.

(a)

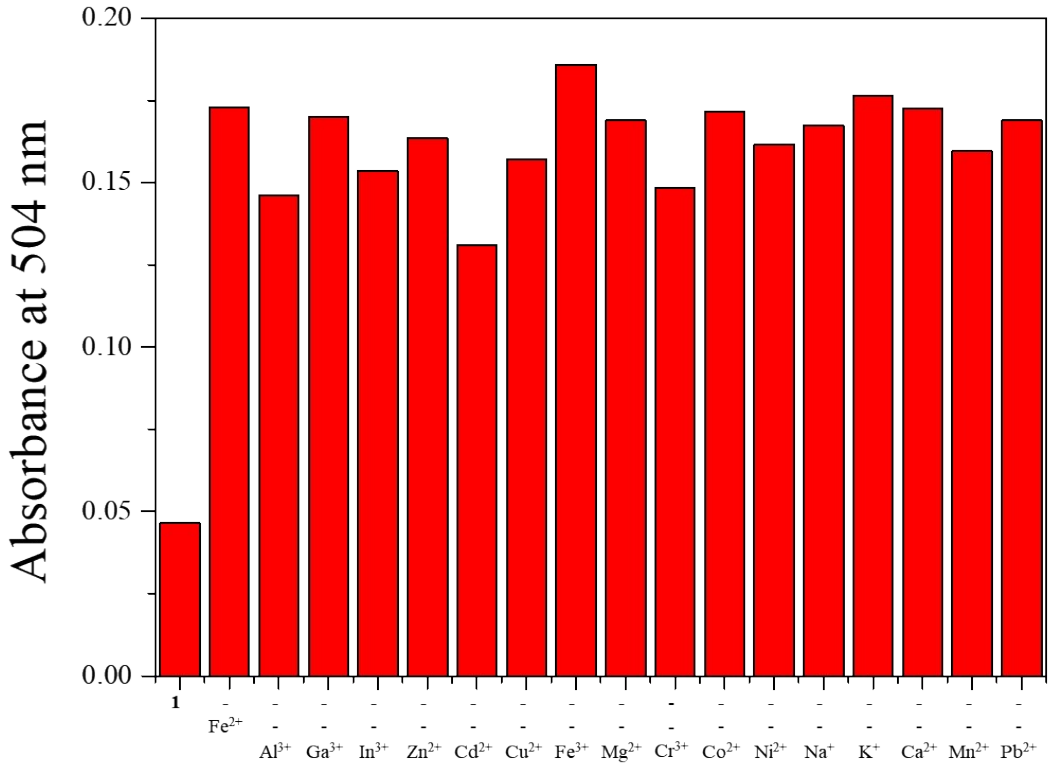

(b)

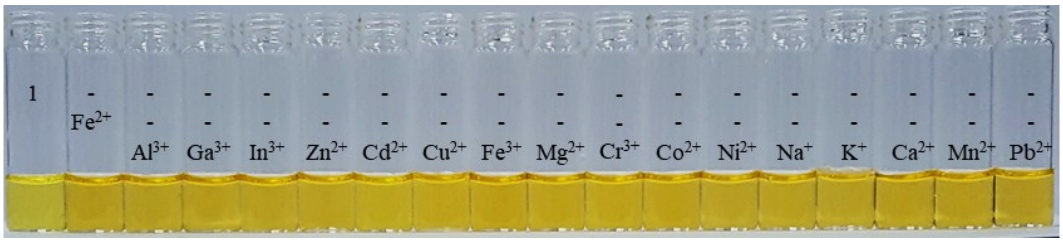

Fig. S13. (a) UV-vis absorption changes (at 490 nm) and (b) the color changes of **1** (30 μM) upon addition of Fe^{2+} (0.5 equiv) in the absence and presence of other metal ions (0.5 equiv).

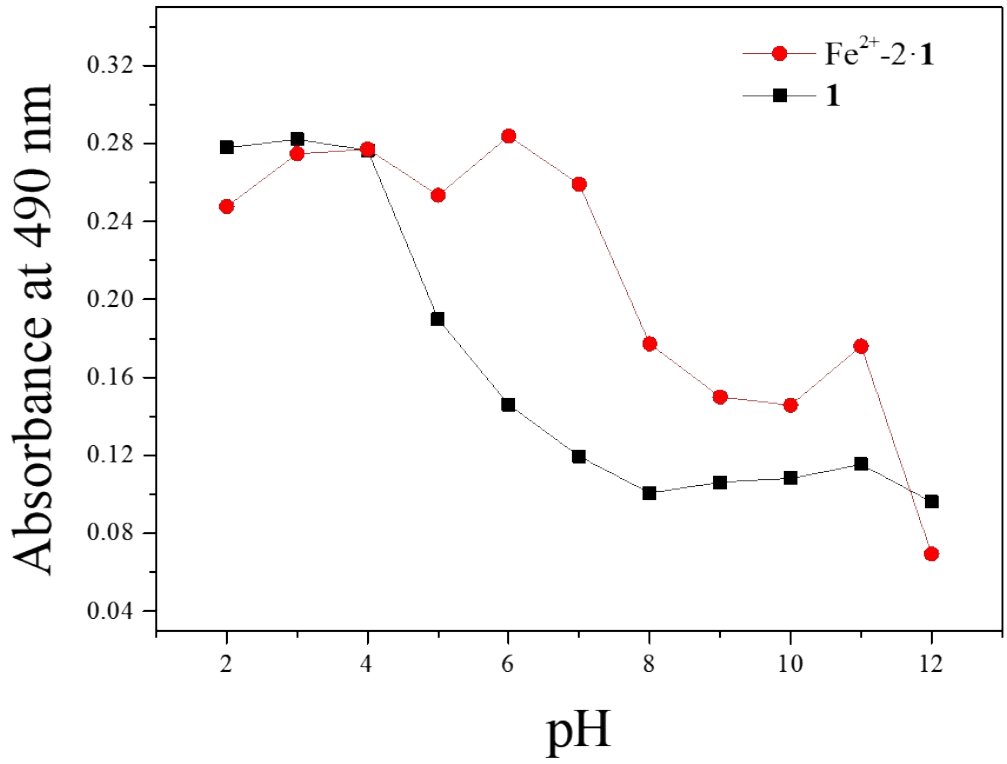

Fig. S14. UV-vis absorbance (at 490 nm) of **1** (30 μM) and Fe^{2+}-2·**1** complex in different pH (2-12) solution (bis-tris buffer, 10 mM), respectively.

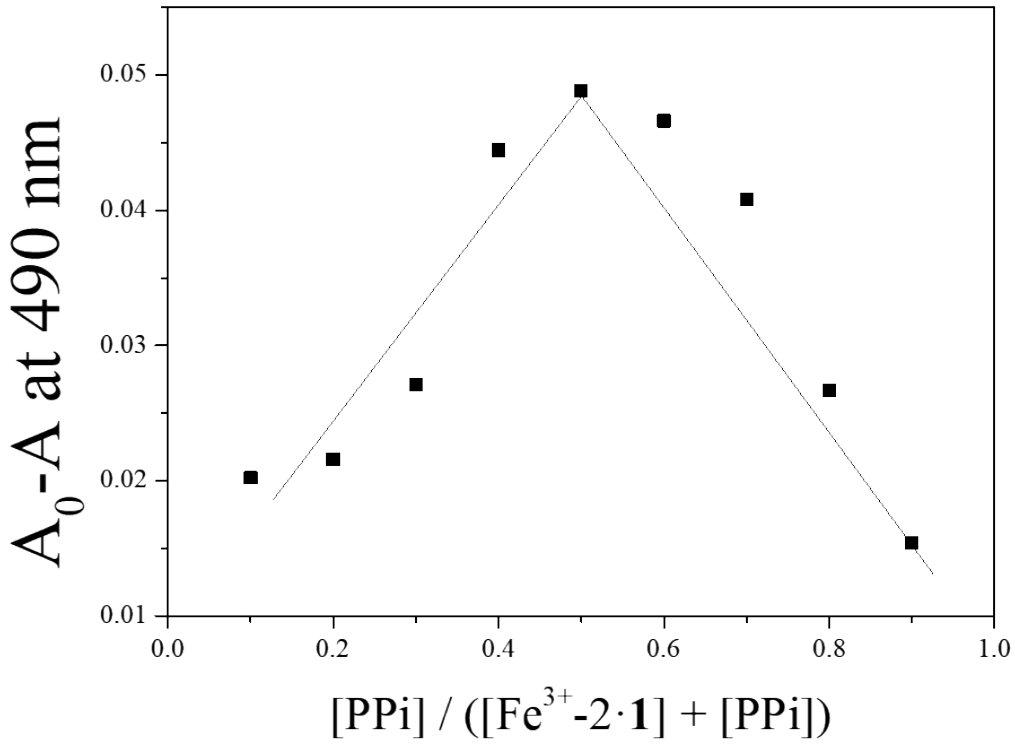

Fig. S15. Job plot of Fe^{3+}-2·**1** complex (40 μM) toward PPi, where the absorbance at 490 nm was plotted against the mole fraction of PPi.

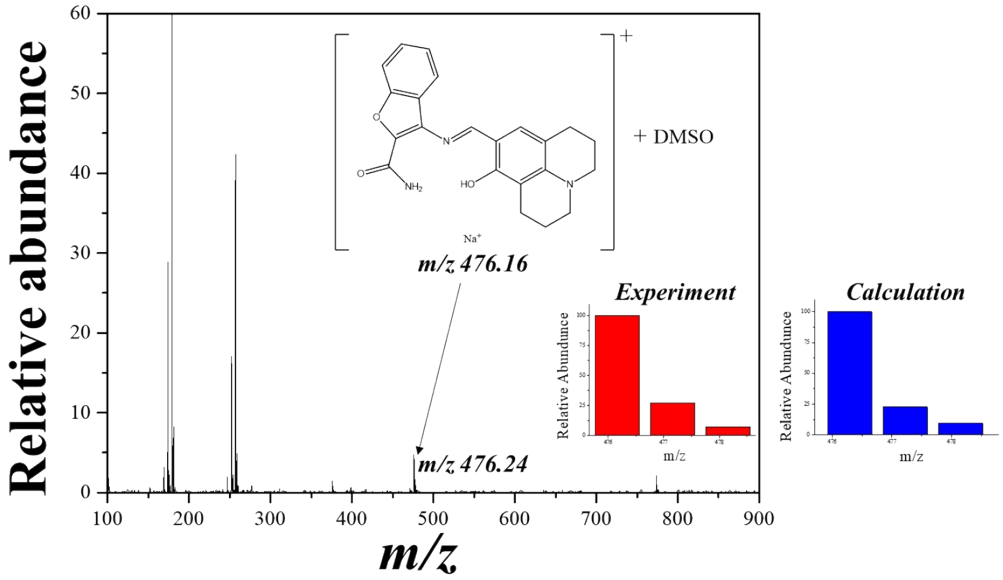

Fig. S16. Positive-ion ESI-mass spectrum of Fe^{3+}-2·**1** (100 μM) upon addition of PPi.

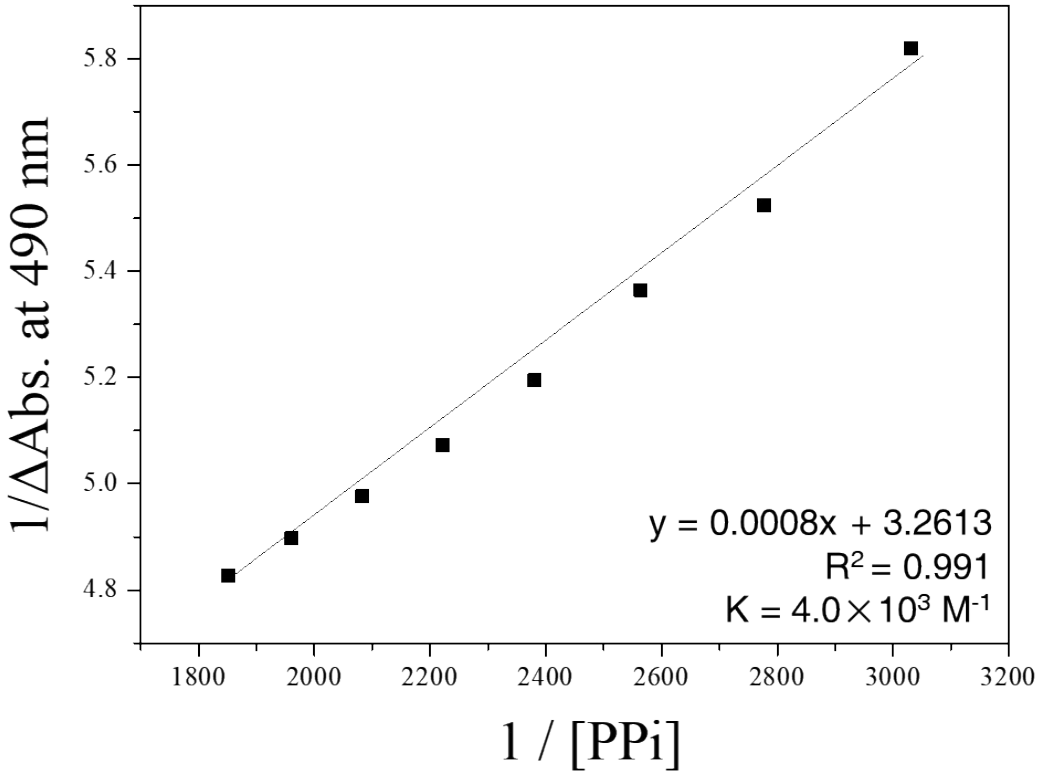

Fig. S17. Benesi-Hildebrand plot of Fe^{3+}-2·**1** (30 μM) for PPi, assuming 1:1 stoichiometry for association of Fe^{3+}-2·**1** with PPi.

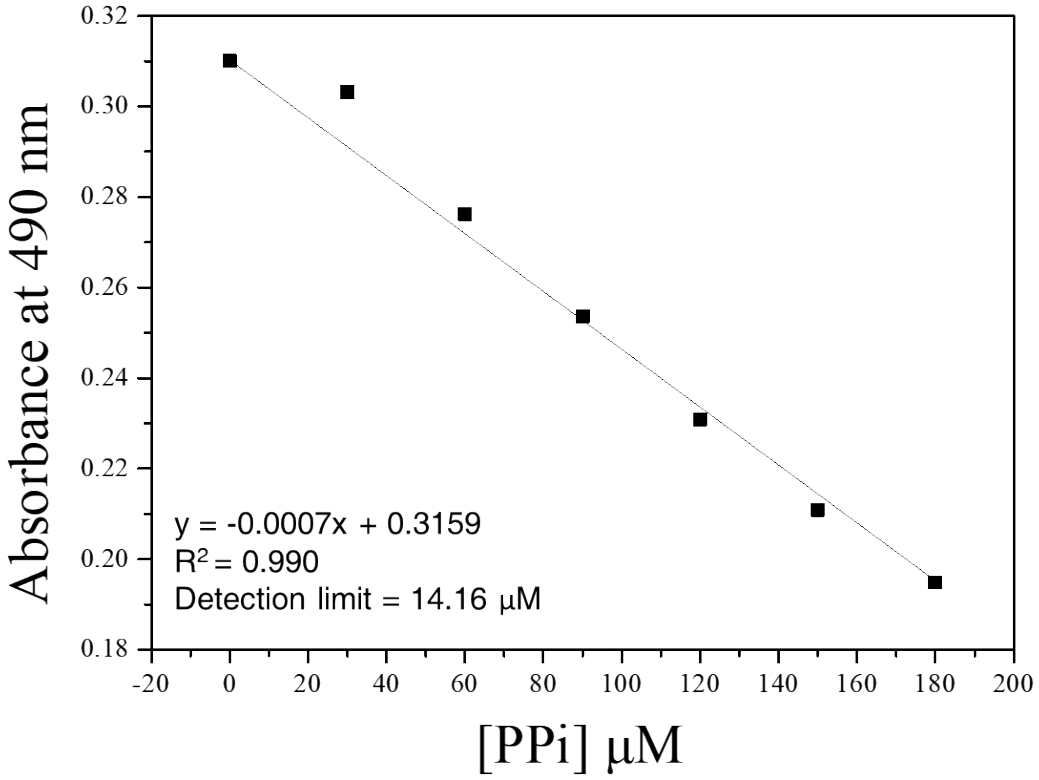

Fig. S18. Determination of the detection limit of Fe^{3+}-2·**1** (30 μM) for PPi based on change of absorbance at 490 nm.

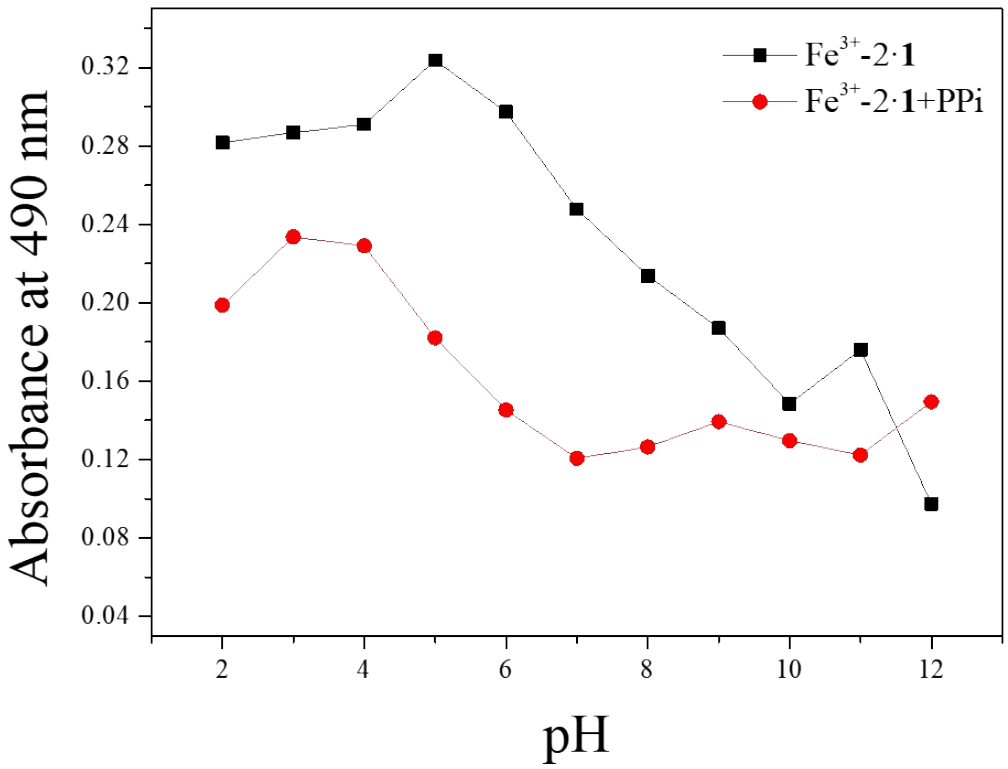

Fig. S19. UV-vis absorbance (at 490 nm) of Fe^{3+}-2·**1** (30 μM) and Fe^{3+}-2·**1**+PPi in different pH (2-12) solution (bis-tris buffer, 10mM), respectively.